# Mobility Characterization and Dynamical Analysis of a Surface Hopper for Low-gravity Environments

Miguel Borges Pinheiro
miguel.pinheiro@ist.utl.pt

Instituto Superior Técnico, Univeridade de Lisboa, Portugal

January 2021

**Abstract**

The growing scientific interest in the exploration of low-gravity celestial bodies, such as asteroids, comets, or small planetary satellites, has developed a higher need for mobile surface missions. Internally-actuated hopping systems provide an efficient and viable opportunity to achieve surface mobility under such environments, with low operational cost. The rover's actuation using flywheels, implements a high control, design flexibility, and enclosed mobility mechanism. Through self-righting maneuvers, fewer actuators are needed and a simpler single-axis hopping motion can be achieved. Throughout this work, the rover's hopping mobility based on these configurations is studied. The dynamics and simulations resulted in innovative proposed implementations to the spike configurations. It is showed the interest of applying a variable spike angle configuration and a variable spike length configuration. The application of a spike that can adjust and control its angle improves significantly the hop distance achieved for different surface inclinations. The implementation of a spike that can change its length works as a trade-off solution between more efficient hops, with shorter spikes, and better transverse capability over higher obstacles, with longer spikes. This later variation presents mainly a potential contribution to the landing stage, however a further study of this application is needed.

**Keywords:** Mobility, Rover, Hopping Dynamics, Small Body Exploration, Spike configuration

## 1. Introduction

The exploration and investigation of small celestial bodies such as small planetary satellites, asteroids, and comets, have been increasing in the last years. These objects may enable to better explain the origin of the universe and the evolution of the solar system. Missions conducted to study asteroids and comets were successful to establish the current understanding of their evolution, characteristics and composition. However, much more investigation is required to fully understand and study these small bodies.

Mobile rovers are specially interesting for the exploration of this small celestial targets as they can move through the surface and perform important operations that allow the better understanding and characterization of these space objects. Their small size and low investment funds needed are very attractive characteristics and could grant the possibility of future missions where several of this robots work together simultaneously. The biggest obstacles of these missions are the complex and varying surface composition and the micro-gravity environment that make surface mobility very challenging.

Relevant missions to Small Bodies were performed throughout the years. Being able to measure important data of comets, small planetary satellites, and asteroids. But it was only in 2018 that the first mobile rovers successfully operated on a small body surface. In 2005, JAXA launched the spacecraft Hayabusa to (25143) Itokawa, which was able to obtain the first successful sample return from an asteroid. However, the mobile rover MINERVA on board of the spacecraft was unsuccessful to reach the asteroid's surface [18]. JAXA's second mission Hayabusa 2 spacecraft, to the target asteroid 162173 Ryugu, successfully deployed mobile rovers on the surface in 2018. The MINERVA-II autonomous hoppers and the MASCOT lander, developed by DLR, successfully performed hops on the surface and retrieved important measurements and data [16].

## 2. Background

First, different mobility approaches and rover configuration designs were considered to determine the desired rover characteristics.

### 2.1. Mobility Approaches

The developed projects of mobile rovers for Small Body exploration have grown exponentially throughout the years, with different approaches to mobility proposed. The main types of mobility can be divided into: wheeled, leg-type, and hopping rovers. On friction-based mobility, according to the Coulomb's law, the driving force is given by:

$$0 \leq F_f \leq \mu F_N \tag{1}$$

Wheeled robots use exclusively the surface normal forces to generate horizontal traction, which is strongly dependent on the gravity ($F_N = mg$). On micro-gravity environments the friction force available for wheeled robots is exceptionally low, leading to extremely low speeds [7]. In addition to the presence of extremely irregular surface, the wheeled rovers do not present a viable solution for the exploration of small bodies.

The leg-type locomotion requires complex actuation and driven mechanisms, together with the high mission duration to transverse long distances. This mechanisms also rely on the surface characteristics that are usually highly unknown, which can result in anchoring challenges, as displayed by Philae's landing on a comet [5].

On another side, hopping rovers use the low-gravity in their favour. This friction-based mobility uses an artificial pulling force applied against the surface to make the rover hop ($F_N = (mg + F_h)$). So even with extremely low gravity levels, hoppers can assure mobility.

### 2.2. Hopping Methods

Different principles and concepts can be used to perform surface mobility by hopping. There are three main principles: *thruster*, repulsion and *torquer* mechanisms. Repulsion mechanisms include elastic and striking methods, with the later referring to hitting the surface with a movable arm or part.

Thursters have a heavy and operationally complex system, they are limited to a finite number of hops, and they represent a possible surface contamination agent. In addition, the low-gravity environment does not require such high thrusting force to perform surface hops. Elastic and striking based mechanisms on the other hand provide virtually "infinite" number of hops and a simpler system approach. The most common configuration lays upon a spring compression mechanism for hopping. This type of mobility was the first to be used in in-situ missions to small bodies, with the PrOP-F Phobos hopping rover onboard of the Phobos 2 spacecraft in 1988. Unfortunately this rover was not able to communicate with the main spacecraft so no performance data was obtained [13]. Several elastic based designs were proposed throughout the years for low-gravity and Moon surface mobility [2, 15, 14, 17, 10]. However, the elastic-based method of hopping represents an abrupt and impulsive actuation which results in a poor control capability of the hop angle and velocity. Also, considering that to perform a hop the rover needs to have the right attitude on the surface it does not represents an admirable adaptability to the irregular terrain.

Alternatively, torquer systems use internally-actuated torque to rotate the hopper and produce a reaction force against the surface to make the rover hop. The thrusting force obtained is much smaller than the spring-based hoppers, which might represent a complication for the mobility on Moon and Mars gravity levels, where a too powerful and heavy torque is needed. However, this is not a problem for micro-gravity environments where the torques needed are significantly much lower. This hopping principle has been widely applied in mobility rovers for surface exploration of small bodies [19, 8, 6]. The main advantage of this type of hoppers is the high control ability. It also possesses higher adaptability to the uneven terrain in comparison to other hopping principles. Since the actuator is inside the body, it is protected against contamination by potential dusts that might be part of the surface. The torquer can also be used to perform attitude control during the hop flight, tumbling motions or to posture the hopper in the right direction to perform the following hop.

### 2.3. Torquer Configurations

Different configurations can be implemented for the torquer mechanism. The MASCOT hopper, developed by the German Aerospace Center (DLR), uses an internal eccentric arm driven by a brushless DC motor [12]. While the rover is on the ground, by accelerating and decelerating the arm in a rotating motion, a defined torque is applied on the hopper by the resulting reaction force. This mechanism allows hopping and self-righting maneuvers in different directions.

Other more used *torquer* methods have been implemented with orthogonal DC motors attached with a mass on a momentum wheel (i.e. a flywheel as a comprised disk). A flywheel consists of a rotating mass that stores kinetic energy. The internal mounted flywheels allow for enough torque to be produced and transfer through acceleration and braking to the hopper's body to perform a hop, alongside with the design flexibility for other instruments inclusion. This internal torque produced by the rotating flywheel can be used to change direction or perform a hop with a controlled speed. Examples of this torquer hopping approach are the MINERVA rover [19], Hedgehog [6], and the Cubli

[3].

Different configurations for the torquers placement can be considered. Symmetric designs with 3-DoF actuators [3] [6], by 3 or more torquers installed, which allow the hopper to hop in any arbitrary direction regardless of its resting position and attitude, however it also implies more actuators and a heavier rover. And configurations with less torquers and only 2-DoF actuators [19], which can still move for any attitude, having however to perform a self-righting operation or adjust its orientation if the initial hopper's position is not the required to execute the next hop.

### 2.4. Selected Configuration

The selected configuration to be studied combines both the Hedgehog and MINERVA principles and approaches [6, 11]. In one hand, the external cubic like shape structure with spikes on its corners, such as the Hedgehog configuration, is used. On the other hand, the internal configuration of two torquers applied by the MINERVA is favored. This requires a self-righting maneuver after the hop and subsequent landing rebounds on the ground, but allows for a simpler process of hopping with a two step motion: a twisting maneuver of directional pointing, and then hopping about a axis parallel to the surface. The aforementioned hopping approach is slower but more controllable and accurate than oblique hopping about inclined axes, enabled by the three orthogonal flywheel configuration of the Hedgehog [6]. DC motors with incorporated flywheels are selected as actuators.

For the hopping initiation and flywheel actuation, it is chosen the control strategy of slowly spinning up the flywheels with a motor torque lower than the one that would make the hopper initiate a rotation, so it remains grounded during the actuation of the flywheels. Then a high-torque mechanical brake is applied when the desired flywheel speed is achieved to initiate the hop. This approach was also used and tested by Hockman et. al [6], and provides fast energy transfer if aggressive hops are requested, represents a simple control strategy, and solves any eventual flywheel saturation problems [1]. This control strategy will be referred from now on as *build-up strategy*.

The selected configuration for this work leverages attitude control during the flight phase. This provides instrument pointing for picture acquisition like MINERVA, but also the ability to control the hopper's direction and pose for the impact landing.

## 3. Dynamics

Under the configuration described the rover's hopping movement is performed about a single axis, controlled by one single flywheel actuation and in which the contact reaction forces with the ground occur about the pair of stance spike tips. This allows a two-dimensional dynamic analysis of the system in a cut-section perspective, as shown in Figure 1. The rover's mass distribution is assumed uniform and his centre of mass coincident with its geometric centre. The hopper is modelled in two-dimensions as a disk with equispaced rigid spikes attached and with a single flywheel driven by a motor at its center of mass, as the commonly used model of passive dynamic walking [9].

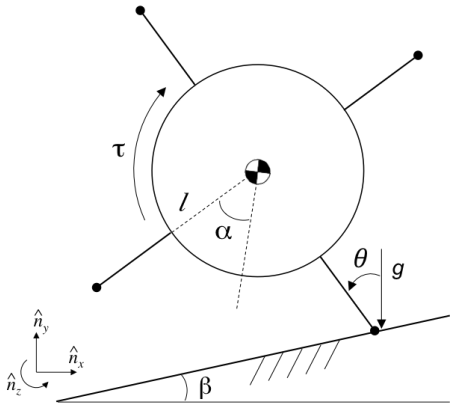


Figure 1: Representation of the hopper's 2D model.

The angle $\theta$ represents the angle between the stance spike tip and the vertical. The angle $\alpha$ is the spike angle. The angle $\beta$ is referred to the surface inclination on the hopper's initial position. The length from the center of gravity to the spike tips is represented by $l$. And $\tau$ is the torque applied on the hopper.

For a first-order representation of the hopper's motion it is acceptable to assume a flat and homogeneous surface, that collisions with the ground are inelastic and impulsive, and that the stance spike acts as a pin joint and does not slip. The hopping controlled motion can be divided into a build-up phase, with the hopper at rest due to the *build-up strategy*, a stride phase, while the hopper is rotating supported by a single spike (or pair of spikes), and a flight phase, when there is no longer contact with the surface and the hopper is in a ballistic trajectory.

Using the Lagrangian principle for no dissipation,

$$\frac{d}{dt}\frac{\partial L}{\partial \dot{q}} - \frac{\partial L}{\partial q} = \frac{\partial \delta W}{\partial \delta q}, \tag{2}$$

with $q = \theta$ and $L = T - V$. From the no-slip assumption, the hopper's linear velocity $v = \sqrt{\dot{x}^2 + \dot{y}^2}$ from its centre of mass is then given by $v = l\dot{\theta}$. With the hopper at rest on the initial position defined by $(x, y) = (0, l\cos\theta)$. Hence,

$$L = \frac{1}{2}(I_r + m_r l^2)\dot{\theta}^2 - m_r g l \cos\theta \tag{3}$$

$$W = -\tau\theta \tag{4}$$

Where $I_r$ is the hopper's rotational inertia and $m_r$ the hopper's total mass. Solving for Equation 2:

$$\ddot{\theta}(t) = \frac{m_r g l \sin\theta(t) - \tau(t)}{I_r + m_r l^2} \tag{5}$$

The equation of motion is that of an inverted pendulum.

From here it is possible to calculated such minimum torque that would make the hopper start the stride phase in a clockwise rotation (i.e. $\ddot{\theta} < 0$). By the schematics of Figure 1, $\theta(0) = (\alpha + \beta)$, and so:

$$\tau_{min} = m_r g l \sin(\alpha + \beta) \tag{6}$$

During the build-up phase it is important that the flywheel generated torque is lower than this torque in Equation 6. The torque generated by the flywheel is defined by:

$$\tau = I_f \dot{\omega}_f \tag{7}$$

Where $I_f$ is the flywheel's rotational inertia and $w_f$ the flywheel's angular speed.

### 3.1. Instantaneous momentum transfer

In the presence of high friction brakes (e.g. pin brakes or impact hammers), where an impulsive braking is applied, the momentum transfer from the rotating flywheel to the hopper can be assumed instantaneous. For this case, there is no applied torque on the rover from the flywheel during the stride phase, which results in only one control input variable (i.e. the flywheel speed), and the equation of motion is defined as:

$$\ddot{\theta}(t) = \frac{m_r g l \sin\theta(t)}{I_r + m_r l^2} \tag{8}$$

The angular momentum of the flywheel prior to the brake is $(I_f \omega_f)$ and the angular momentum of the hopper about the stance spike tip immediately after the brake is given by $(I_r \dot{\theta}_0 + l m_r v_0)$. Due to the assumption of the spike tip behaving as a pin joint $v = l\dot{\theta}$, by the conservation of angular momentum principle it is obtained:

$$\dot{\theta}_0 = \frac{I_f \omega_f}{I_r + m_r l^2} \tag{9}$$

This represents the angular velocity of the hopper in the instant immediately after the momentum transfer (i.e. in the beginning of the stride phase, $t = 0$). The stride phase begins immediately after the momentum transfer, meaning the hopper's angle $\theta$ in that instant $(t = 0)$ is then given by:

$$\theta_0 = \alpha + \beta \tag{10}$$

From an energy transfer point of view, initially there is the flywheel kinetic energy just before the brake:

$$E(t^-) = \frac{1}{2} I_f \omega_f^2 \tag{11}$$

And immediately after the brake the resulting hopper's kinetic energy:

$$E(t^+) = \frac{1}{2}(I_r + m_r l^2)\dot{\theta}_0^2. \tag{12}$$

Which allows to obtain the correspondent energy transfer efficiency:

$$\eta = \frac{E(t^-)}{E(t^+)} = \frac{I_f}{I_r + m_r l^2} \tag{13}$$

### 3.2. Momentum transfer not instantaneous

In the presence of other types of brakes, such as friction disks and band brakes, like the one used and determined as the most effective and reliable by Stanford in the Hedgehog hopper [6], momentum transfer can not be considered instantaneous. In this braking systems a constant braking torque is applied $\overline{\tau}$ for a $\Delta t$ time duration of braking until the flywheel comes to a full stop. As shown by Hockman et. al [6], this relation can be written and described by:

$$\overline{\tau}\Delta t = I_f \omega_f \tag{14}$$

For this case, the equation of motion is defined as:

$$\ddot{\theta}(t) = \frac{m_r g l \sin\theta(t) - \overline{\tau}}{I_r + m_r l^2} \tag{15}$$

If aggressive hops are considered, with high enough torque applied such that it is possible to assume that $\overline{\tau} >> m_r g l \sin\theta$, this means Equation 15 can be simplified into a linear second order ordinary differential equation:

$$\ddot{\theta}(t) = \frac{-\overline{\tau}}{I_r + m_r l^2} \tag{16}$$

Which allows, through integration, to obtain the analytical expected angular velocity and angle through time. Knowing the initial state is determined by $\dot{\theta}(0) = 0$ and $\theta(0) = \alpha + \beta$, this results in:

$$\dot{\theta}(t) = \frac{-\overline{\tau}}{I_r + m_r l^2} t \tag{17}$$

$$\theta(t) = \frac{1}{2}\frac{-\overline{\tau}}{I_r + m_r l^2} t^2 + \alpha + \beta \tag{18}$$

For other hops, Equation 15 must be solved numerically.

3.3. Condition to perform a hop

The dynamical condition to perform a hop is given by the loss of ground contact, which means the normal contact force $R_N$ crosses from positive to zero marking the end of the stride phase and the beginning of the flight. Analyzing the free-body diagram of the system and solving its equations, this condition is given at the hopping instant ($t_h$) by:

$$\dot{\theta}^2(t_h) > \frac{g\cos\beta}{l\cos\left(\theta(t_h)-\beta\right)} - \ddot{\theta}(t_h)\tan\left(\theta(t_h)-\beta\right) \tag{19}$$

3.4. Flight Phase

The flight phase of the hopping motion follows a straight ballistic trajectory. The initial state of this phase is described by the hopping instant determined by the end of the stride phase. From this known movement it is possible to obtain the resulting expected horizontal distance achieve by the hop:

$$d_h = \frac{v_h^2}{g}\sin(2\theta_h), \quad \text{with} \quad v_h = l\dot{\theta}_h \tag{20}$$

3.5. Contact Model

The contact dynamics are present in different separate stages of the hopper's operation. While the hopper is performing a controlled motion in continuous contact with the surface (i.e. stride phase), and on collisions with the ground at landing. The two different cases are studied separately, as they represent different dynamic situations and interactions.

The contact model during the stride phase will be considered as a 2-DoF system composed by a Coulomb friction component tangential to the surface, and a spring-damper component that is normal to the surface [4]. The normal contact force represented by the spring-damper system is given by:

$$F_n = -Ky_c - C\dot{y}_c \tag{21}$$

With $K$ and $C$ representing respectively the surface stiffness and damping parameters. And with $y_c$ representing the spike vertical position relative to the surface. The associated contact potential energy from the spike penetrating $y_c$ into the elastic surface, and the contact dissipative energy from the spike being actively penetrating the surface, are defined as:

$$V_c = \frac{1}{2}Ky_c^2, \quad \text{for } y_c \leq 0 \tag{22}$$

$$D_c = \frac{1}{2}C{\dot{y}_c}^2, \quad \text{for } \dot{y}_c < 0 \tag{23}$$

The hopper's center of mass position $(x, y)$ can be written as:

$$y = y_c + l\cos\theta \tag{24}$$

$$x = l\sin\left(\alpha+\beta\right) - l\sin\theta \tag{25}$$

Using the Lagrangian approach, with $q = (y_c, \theta)$:

$$\frac{d}{dt}\frac{\partial T}{\partial \dot{q}} - \frac{\partial T}{\partial q} + \frac{\partial D}{\partial \dot{q}} + \frac{\partial V}{\partial q} = \frac{\partial \delta W}{\partial \delta q} \tag{26}$$

The resulting system of equation that govern this motion is given by:

$$\begin{cases} m_r(\ddot{y}_c - \ddot{\theta}l\sin\theta - \dot{\theta}^2 l\cos\theta) + C\dot{y}_c + Ky_c + m_r g = 0 \\ (m_r l^2 + I_r)\ddot{\theta} - \ddot{y}_c m_r l\sin\theta - m_r g l\sin\theta = -\tau \end{cases} \tag{27}$$

## 4. Simulations and Results

The numerical integration of the equations of motion is performed using a fifth-order Runge-Kutta integrator method, programmed using the MATLAB software. The design parameters used are the ones of the Hedgehog rover [6], listed in Table 1. The surface parameters used for the simulations are: surface stiffness $K = 10000\ [N/m]$, surface damping $C = 1000\ [Ns/m]$.

| Parameters | Definition |
|---|---|
| $m_r = 2.3\ kg$ | Total mass |
| $I_r = 0.013\ kg{\cdot}m^2$ | Rotational inertia |
| $l = 0.168\ m$ | Spikes' length from CG |
| $\alpha = \pi/4\ rad$ | Spike angle |
| $I_f = 9.5 \times 10^{-4}\ kg{\cdot}m^2$ | Flywheel's inertia |
| $g = 5.8 \times 10^{-3}\ m/s^2$ | Phobos' gravitation |

Table 1: Hedgehog mission parameters [6].

4.1. Instantaneous momentum transfer brake

The control input variable in this case is only the flywheel speed prior to the braking.

The initial states for the equations of motion determined by Equation 27, with $\tau = 0$, are described as:

$$Y = \begin{bmatrix} y_c \\ \theta \\ \dot{y_c} \\ \dot{\theta} \end{bmatrix} \quad Y_0 = \begin{bmatrix} -0.0001 \\ \alpha+\beta \\ 0 \\ \frac{I_f\omega_f}{I_r+m_r l^2} \end{bmatrix} \tag{28}$$

The simulation results, represented in Figures 2 and 3, show that for an instantaneous momentum transfer scenario, it is safe to assume that the stride phase duration is zero for any flywheel initial speed. And that the flight phase initiates immediately after the momentum transfer. This results in $t_h \equiv t_0$, hence the correspondent hopping angle and hopping angular speed are given by:

$$\theta_h = \alpha + \beta, \qquad \dot{\theta}_h = \frac{I_f\omega_f}{I_r + m_r l^2} \tag{29}$$

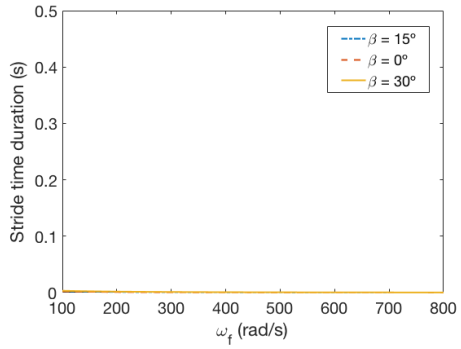


Figure 2: Duration of the stride phase in terms of the flywheel speed.

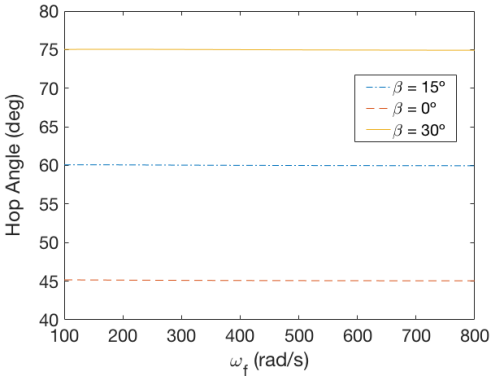


Figure 3: Hop angle as function of the flywheel speed.

In this regime, Equation 29 demonstrates that the hopping angle is determined solely by the spike geometry and the surface inclination. From Equation 20, provided by the ballistic flight trajectory, the lateral distance is maximized for a hopping angle of 45°. Facing different surfaces inclinations through the hopper's mobility operations, this optimised angle can only be achieve or approached in all occasions with a spike configuration of variable angle ($\alpha$).

From these results and the known flight ballistic trajectory, it is possible to write the flywheel's initial rotational speed $\omega_f$ as function of a desired hopping distance:

$$\omega_f(d_h) = \sqrt{\frac{d_h g}{\eta^2 l^2 \sin(2(\alpha+\beta))}} \tag{30}$$

Allowing to obtain the viability of such hopping system in terms of the gravity levels, for a $50m$ horizontal hop, as shown in Figure 4.

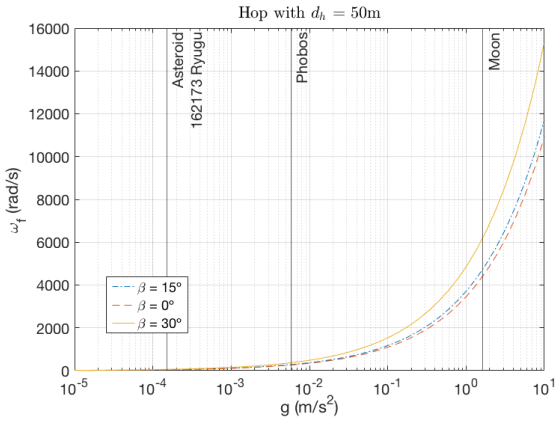


Figure 4: Required flywheel speed as function of the gravitational acceleration.

The results support that the presented hopper's mobility is only viable for low-gravity bodies. As Figure 4 demonstrates, for a hopper with the Hedgehog design, the feasible flywheel speed generated is only viable for gravity levels of $10^{-5}$ to $10^{-2}$ $m/s^2$ [6].

### 4.2. Constant torque braking

With a constant brake ($\overline{\tau}$) being applied until the flywheel comes to a complete stop, the initial state for the equations of motion determined by Equation 27, in this case is defined by:

$$Y = \begin{bmatrix} y_c \\ \theta \\ \dot{y_c} \\ \dot{\theta} \end{bmatrix} \quad Y_0 = \begin{bmatrix} -0.0001 \\ \alpha+\beta \\ 0 \\ 0 \end{bmatrix} \tag{31}$$

Several simulations were performed for this case, which demonstrated interesting results, as shown in Figures 5 to 10. The stride duration is in agreement with the expected dynamic analysis. The braking torque influence on the hop angle and hop distance for high torques is also in agreement with the analytical model for aggressive hops.

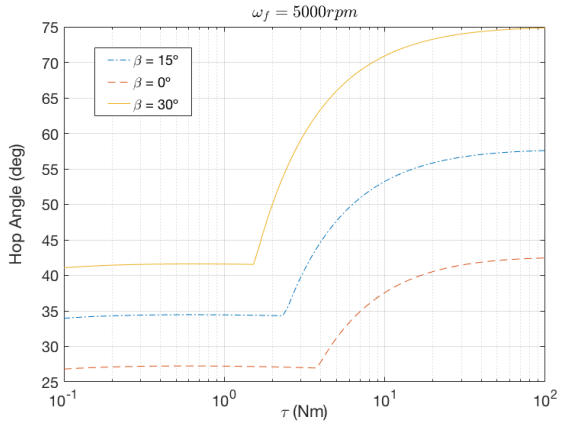


Figure 5: Hop angle with constant braking torque for a flywheel speed of 5000rpm and Hedgehog parameters.

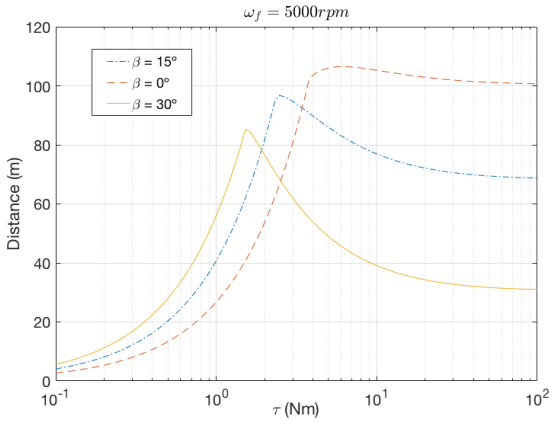


Figure 8: Hop Distance with constant braking torque for a flywheel speed of 5000rpm and Hedgehog parameters.

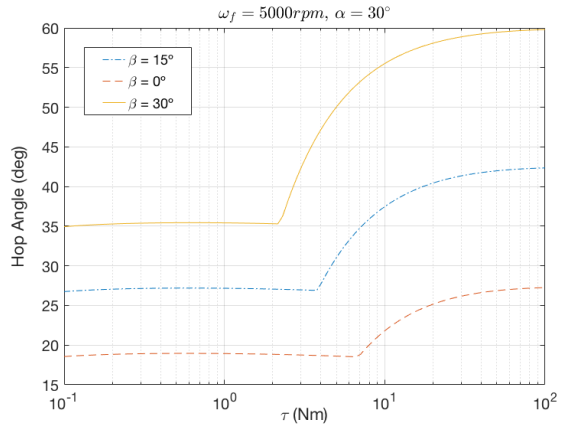


Figure 6: Hop angle with constant braking torque for a flywheel speed of 5000rpm and an adjusted 30 degree spike angle.

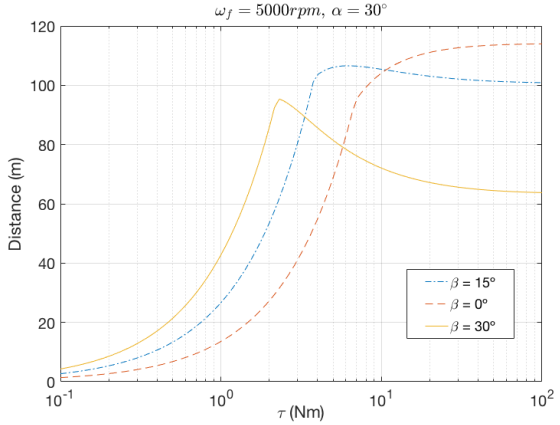


Figure 9: Hop Distance with constant braking torque for a flywheel speed of 5000rpm and an adjusted 30 degree spike angle.

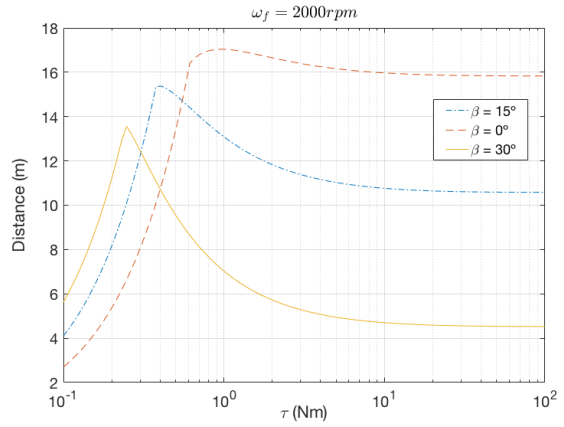


Figure 7: Hop Distance with constant braking torque for a flywheel speed of 2000rpm and Hedgehog parameters.

The simulations show the high influence of the flywheel initial speed on the hop distance achieved by the hopper, as visible by comparing Figure 7 and 8. The constant braking torque applied to the flywheel has significant influence in the hop angle and hop distance obtained. The point on the curves where there is a change of behaviour marks the constant torque value $\overline{\tau}$ from which the flywheel is fully stopped before the stride phase comes to an end. Prior to that torque value, the flight phase is initiated before the flywheel comes to a complete stop. Torque brakes above that point are favored, considering it not only simplifies the actuation input for the hop to the flywheel speed prior to the brake, but also allows for all the momentum generated on the flywheel during the build-up phase to be used for the hop.

From Figures 7 and 8, it is visible that after the aforementioned changing point, when in the

presence of surface inclination $\beta$, the hopping distance achieved decreases until it starts converging for higher torque values. This is a result of the hopping angle deviation from its desired value of 45°, which does not happen in the case where there is no surface inclination (i.e. $\beta = 0°$), as shown in Figure 5. This can be solved by the implementation of an angle adjusting mechanism on the spikes, actuated when the hopper is standing with inclination. Figure 9 shows the resultant changes in the hop distance when adjusting the spike angle to 30° instead of the 45° fixed angle used in the Hedgehog. In the presence of surface inclination, for both $\beta = 15°$ and $\beta = 30°$, it shows clear improvement on the hop distance obtained for higher torque brakes, comparing with the results of Figure 8. For the surface inclination of $\beta = 15°$, the hop distance achieved by the adjusted spike angle to $\alpha = 30°$ is improved between 30% to 45%, for high torque values between 6 and 100 Nm. As also supported by Figure 6, where for a spike angle of 30° and surface inclination of 15°, the hop angle for higher torques is closer to the 45° for maximized hopping distance. These results represent evidences of the interest of studying the implementation of spikes that variate their angle, and consequently adjust and adapt to different surface inclination and conditions.

The simulations performed with an increased spike length, in comparison to the one used in the Hedgehog prototype, support the analytical conclusion that shorter spikes provide better efficient hops. Figure 10 represents an example for a length $l = 22.6cm$, and demonstrates the decrease of the hop distance achieved.

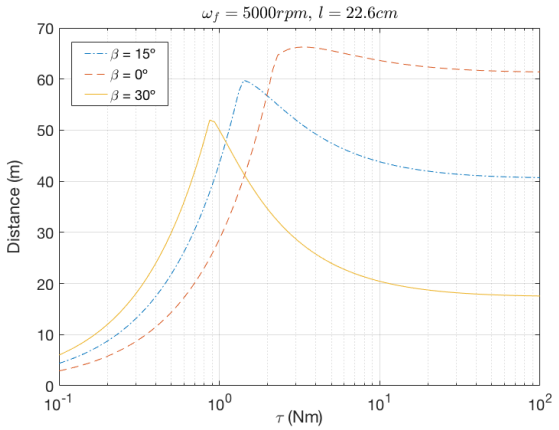


Figure 10: Hop Distance with constant braking torque for a flywheel speed of 5000rpm and an adjusted spike length to l=22.6cm.

## 5. Conclusions

Through this work a viable hopping rover configuration was selected and its dynamics studied. The simulation results alongside with the dynamical analysis support the interest of applying a spike configuration with a variable angle, as demonstrated by Equations 18 and 29, and by the plotted results. The implementation of a variable length spike configuration presents an interesting trade-off solution between the better efficiency and longer hop distance achieved with shorter spikes, and the better transverse capability of bigger obstacles with longer spikes. It also represents an appealing potential improvement to the landing envelope, with the application of an internal damping system on the retractable spikes that provides a energy dissipation mechanism for the impact.

The proposed ideas for spike implementations create an opportunity of future work, to study and develop effective, simplistic and robust mechanisms to apply such configurations. And in a second level of the project development, test and conduct experiments to a constructed prototype.

As an improvement to the work developed is suggested a second-order dynamic analysis for the inclusion of potential slipping motions on the hopping initiation. The landing simulations are left for future work considering it would be leveraged a more complex contact model, using Multi-Body-System simulation software or a high-fidelity Digital Elevation Models (DEM). This would allow to simulate the hopper impacts at different velocities and attitudes upon landing, and obtained a high-reliable reproduction of the expected movements and behaviour of the hopper on the irregular surface. Providing a favorable testing for the proposed damping landing idea implemented on the retractable spikes.

The overall objectives of this work were achieved and important potential new implementations to the hopper's mobility system emerged. Leaving space and a opportunity for further development and study of this work.


## Acknowledgements

A word of appreciation to my supervisors at Técnico Lisboa, Professors Rodrigo Ventura and João Oliveira, for the opportunity of working on this topic.

The author sincerely thanks Dr. Benjamin J. Hockman (JPL), for the insightful discussion and advice over the topic and work performed.


## References


[1] R. Allen, M. Pavone, C. McQuin, I. A. Nesnas, J. C. Castillo-Rogez, T. N. Nguyen, and J. A. Hoffman. Internally-actuated rovers for all-access surface mobility: Theory and experimentation. *Proceedings - IEEE International Conference on Robotics and Automation*, pages 5481–5488, 2013.

[2] J. Burdick and P. Fiorini. Minimalist Jumping Robots for Celestial Exploration. *The International Journal of Robotics Research*, 22(7-8):653–674, 2003.

[3] M. Gajamohan, M. Merz, I. Thommen, and R. D'Andrea. The Cubli: A Cube that can Jump up and Balance. *IEEE International Conference on Intelligent Robots and Systems*, pages 3722–3727, 2012.

[4] G. Gilardi and I. Sharf. Literature survey of contact dynamics modelling. *Mechanism and Machine Theory*, 37(10):1213–1239, 2002.

[5] E. Hand. Philae probe makes bumpy touchdown on a comet. *Science*, 346(6212):900–901, 2014.

[6] B. J. Hockman, A. Frick, R. G. Reid, I. A. Nesnas, and M. Pavone. Design, Control, and Experimentation of Internally-Actuated Rovers for the Exploration of Low-gravity Planetary Bodies. *Journal of Field Robotics*, 34(1):5–24, 2017.

[7] R. Jones and B. Wilcox. The MUSES CN rover and asteroid exploration mission. *22nd International Symposium on Space Technology and Science*, pages 2403–2410, 2000.

[8] C. Lange, T. M. Ho, C. D. Grimm, J. T. Grundmann, C. Ziach, and R. Lichtenheldt. Exploring small bodies: Nano- and microlander options derived from the Mobile Asteroid Surface Scout. *Advances in Space Research*, 62(8):2055–2083, 2018.

[9] T. McGeer. *Passive dynamic walking*. PhD thesis, School of EnginSimon Fraser University, 1990.

[10] S. Montminy, E. Dupuis, and H. Champliaud. Mechanical design of a hopper robot for planetary exploration using SMA as a unique source of power. *Acta Astronautica*, 62(6-7):438–452, 2008.

[11] R. G. Reid, L. Roveda, I. A. D. Nesnas, and M. Pavone. Contact Dynamics of Internally-Actuated Platforms for the Exploration of Small Solar System Bodies. *i-SAIRAS*, pages 1–9, 2014.

[12] J. Reill, H.-J. Sedlmayr, S. K. P. Neugebauer, M. Maier, A. Gibbesch, B. Schäfer, and A. Albu-Schaeffer. Development of a Mobility Drive Unit for Low Gravity Planetary Body Exploration. *ASTRA - 12th ESA Symposium on Advanced Space Technologies for Robotics and Automation*, 2013.

[13] R. Z. Sagdeev and A. V. Zakharov. Brief history of the Phobos mission. *Nature*, 341(6243):581–585, 1989.

[14] S. Shimoda, T. Kubota, and I. Nakatani. New mobility system based on elastic energy under microgravity. *Proceedings - IEEE International Conference on Robotics and Automation*, 3(August 2014):2296–2301, 2002.

[15] S. Shimoda, A. Wingart, K. Takahashi, T. Kubota, and I. Nakatani. Microgravity Hopping Robot with Controlled Hopping and Landing Capability. *IEEE International Conference on Intelligent Robots and Systems*, 2003.

[16] Y. Tsuda, T. Saiki, F. Terui, S. Nakazawa, M. Yoshikawa, and S. ichiro Watanabe. Hayabusa2 mission status: Landing, roving and cratering on asteroid Ryugu. *Acta Astronautica*, 171(January):42–54, 2020.

[17] K. Yoshida. The Jumping Tortoise: A Robot Design for Locomotion on Micro Gravity Surface. *Proceedings of the 5th International Symposium on Artifical Intelligence, Robotics and Automation in Space*, 1999:705–707, 1999.

[18] T. Yoshimitsu, T. Kubota, and I. Nakatani. MINERVA rover which became a small artificial solar satellite. *20th Annual AIAA/USU Conference on Small Satellites*, 2006.

[19] T. Yoshimitsu, T. Kubota, I. Nakatani, T. Adachi, and H. Saito. Micro-hopping robot for asteroid exploration. *Acta Astronautica*, 52(2-6):441–446, 2003.